Published in final edited form as:

*Nature*. 2010 January 7; 463(7277): 108–112. doi:10.1038/nature08650.

# Ligand-specific regulation of the extracellular surface of a G protein coupled receptor

**Michael P. Bokoch**[1], **Yaozhong Zou**[1], **Søren G. F. Rasmussen**[1], **Corey W. Liu**[2], **Rie Nygaard**[1], **Daniel M. Rosenbaum**[1], **Juan José Fung**[1], **Hee-Jung Choi**[1,3], **Foon Sun Thian**[1], **Tong Sun Kobilka**[1], **Joseph D. Puglisi**[2,3], **William I. Weis**[1,3], **Leonardo Pardo**[4], **R. Scott Prosser**[5], **Luciano Mueller**[6], and **Brian K. Kobilka**[1]

[1]Department of Molecular and Cellular Physiology, Stanford University School of Medicine, Stanford, CA 94305

[2]Stanford Magnetic Resonance Laboratory, Stanford University School of Medicine, Stanford, CA 94305

[3]Department of Structural Biology, Stanford University School of Medicine, Stanford, CA 94305

[4]Laboratori de Medicina Computacional, Unitat de Bioestadística, Universitat Autònoma de Barcelona, Barcelona, Spain

[5]Department of Chemistry, University of Toronto, UTM, Mississauga, Ontario, L5L 1C6, Canada

[6]Bristol-Myers Squibb Pharmaceutical Research Institute, Princeton, NJ 08543

## Abstract

G protein coupled receptors (GPCRs) are seven transmembrane proteins that mediate the majority of cellular responses to hormones and neurotransmitters. They are the largest group of therapeutic targets for a broad spectrum of diseases. Recent crystal structures of GPCRs1,2,3,4,5 reveal structural conservation extending from the orthosteric ligand binding site in the transmembrane core to the cytoplasmic G protein coupling domains. In contrast, the extracellular surface (ECS) of GPCRs is remarkably diverse, and therefore represents an ideal target for the discovery of subtype-selective drugs. However, little is known about the functional role of the ECS in receptor activation, or about conformational coupling of this surface to the native ligand binding pocket. Here we use NMR spectroscopy to investigate ligand-specific conformational changes around a



Correspondence and requests for materials should be addressed to B.K.K. (kobilka@stanford.edu)..

**Author Contributions** M.P.B. designed experiments, purified, labeled and functionally characterized $\beta_2$AR, collected and analyzed NMR data, and wrote the paper; Y.Z. made, expressed and purified $\beta_2$AR lysine mutants, and collected NMR data; S.G.F.R. expressed and purified $\beta_2$AR, and crystallized the $^{13}$C-methylated $\beta_2$AR-Fab complex; C.W.L. designed, optimized and supervised NMR experiments, and collected NMR data; D.M.R., H.J.C, B.I.W. collected diffraction data and refined the structure of the $^{13}$C-Methylated $\beta_2$AR-Fab complex; R.N. collected and analyzed NMR data, and optimized data processing; J.J.F performed G protein coupling assays on labeled $\beta_2$AR; F.S.T. prepared insect cell cultures and purified $\beta_2$AR; T.S.K. purified $\beta_2$AR; J.D.P. advised NMR spectroscopy experiments; L.P. performed molecular modeling and molecular dynamics simulations; R.S.P. designed and optimized NMR experiments, wrote NMR pulse sequences and collected data; L.M. conceived of lysine methylation of the $\beta_2$AR, wrote NMR pulse sequences and designed NMR experiments; B.K.K. supervised the overall project, designed experiments, collected diffraction data and wrote the paper.

**Supplementary Information** is linked to the online version of the paper at www.nature.com/nature

Coordinates and structure factors for [$^{13}$C]methyl-$\beta_2$AR / Fab5 are deposited in the Protein Data Bank (accession code 3KJ6).

central structural feature in the ECS of the $\beta_2$ adrenergic receptor: a salt bridge linking extracellular loops (ECLs) 2 and 3. Small molecule drugs that bind within the transmembrane core and exhibit different efficacies towards G protein activation (agonist, neutral antagonist, and inverse agonist) also stabilize distinct conformations of the ECS. We thereby demonstrate conformational coupling between the ECS and the orthosteric binding site, showing that drugs targeting this diverse surface could function as allosteric modulators with high subtype selectivity. Moreover, these studies provide new insight into the dynamic behavior of GPCRs not addressable by static, inactive-state crystal structures.

---

In the ligand-free basal state, GPCRs exist in an equilibrium of conformations6. Ligand binding modulates receptor function by stabilizing different intramolecular interactions and establishing a new conformational equilibrium. Activating ligands (agonists) stabilize receptor conformations that increase signaling through G proteins; inhibiting ligands (inverse agonists) stabilize other conformations that decrease the basal, agonist-independent level of signaling (Supplementary Fig. 1). When a GPCR is activated, structural changes occur in the cytoplasmic G protein coupling domains. These changes have been characterized for several receptors, including rhodopsin7,8,9,10 and the $\beta_2$ adrenergic receptor ($\beta_2$AR)11,12,13. Recent solid-state NMR data show that light activation of rhodopsin also induces conformational changes in ECL214. In rhodopsin, ECL2 forms a structured cap over the covalently-bound ligand retinal and interacts with transmembrane (TM) segments involved in activation. However, little is known about the effects of diffusible ligand binding on the extracellular domains of other Family A GPCRs, where ECL2 is displaced away from the ligand binding pocket. Here we show that ligands known to differentially affect cytoplasmic domain conformation also stabilize distinct ECS conformations (Supplementary Fig. 1).

Understanding conformational changes in the ECS of GPCRs may provide new avenues for drug design. Comparing the crystallographically identified orthosteric binding pockets of $\beta_2$AR and $\beta_1$AR reveals that 15 of 16 amino acids (94%) are identical1,5. This observation underscores the challenge of identifying subtype-selective drugs for families containing several closely-related receptors (e.g., adrenergic, serotonin, or dopamine receptors)15. In contrast, while the backbone structure of the $\beta_2$AR and $\beta_1$AR extracellular domains are similar, 22 of 39 residues (56%) in ECLs 2 and 3 differ. Therefore, the ECS provides a diverse site for the development of subtype-selective drugs.

The majority of the $\beta_2$AR ECS consists of ECL2, connecting TMs 4 and 5, and ECL3, connecting TMs 6 and 7 (Figure 1a)1,2. ECL2 forms a two-turn $\alpha$-helix that is displaced away from the ligand binding site entrance (Fig. 1b). Two disulfide bonds stabilize ECL2, one within the loop and one to the end of TM3. A salt bridge formed by Lys305$^{7.32}$ and Asp192$^{ECL2}$ connects ECL3-TM7 to ECL2 (superscripts indicate Ballesteros-Weinstein numbering for conserved GPCR residues)16. Carazolol is an inverse agonist that binds in the orthosteric pocket formed by transmembrane segments (TMs) 3, 5, 6, and 7. The only direct interaction between the ECS and carazolol is through an aromatic interaction with Phe193$^{ECL2}$. Given these specific associations between ECLs, the orthosteric ligand binding

site, and TMs involved in activation17, we hypothesized that $\beta_2$AR extracellular domains and the associated salt bridge rearrange upon activation.

To monitor the environment around the Lys305-Asp192 salt bridge by NMR, we selectively carbon-13 labeled lysine side chains in a modified $\beta_2$AR ($\beta_2$AR365) by reductive methylation18 (see Scheme 1, Methods Summary, Supporting Methods, Supplementary Figs. 2-4 and Supplementary Table 1). This approach exploits the sensitivity of methyl groups as NMR probes for analysis of large protein structure and dynamics19. Reductive methylation adds two [$^{13}$C]methyl groups to the ε-$NH_2$ of lysine side chains and the α-$NH_2$ at the receptor amino terminus. The [$^{13}$C]dimethyllysines serve as conformational probes in two-dimensional $^1$H-$^{13}$C correlation NMR experiments. Dimethylation does not alter the lysine positive charge (Scheme 1) and causes little structural perturbation20. We observed no significant changes between the crystal structure of a methylated-$\beta_2$AR/Fab complex bound to carazolol and that of the non-methylated receptor (Supplementary Fig. 5 and Supplementary Table 2). Reductively [$^{13}$C]methylated $\beta_2$AR ([$^{13}$C]methyl-$\beta_2$AR) has ligand binding properties identical to unlabeled $\beta_2$AR, and G-protein coupling is unimpaired (Supplementary Fig. 6).

$$\mathrm{R}-\ddot{N}\mathrm{H}_2 \rightleftharpoons \mathrm{R}-\overset{+}{\ddot{\mathrm{N}}}\mathrm{H}_3 \xrightarrow[NaBH_3CN]{^{13}CH_2O} \mathrm{R}-\ddot{\mathrm{N}}\left(^{13}CH_3\right)_2 \rightleftharpoons \mathrm{R}-\overset{+}{\ddot{\mathrm{N}}}\mathrm{H}\left(^{13}CH_3\right)_2 \quad [1]$$

Intense peaks from dimethylamines (dimethyllysines and the dimethyl-amino terminus) are observed in the $^1$H-$^{13}$C NMR spectrum of [$^{13}$C]methyl-$\beta_2$AR bound to the inverse agonist carazolol in detergent buffer (Fig. 2, dimethylamine region; Supplementary Fig. 7, full spectral width). We used both HSQC and saturation transfer differencing (STD)-filtered HMQC pulse sequences throughout this work; STD-filtered HMQC improved spectral quality at the expense of longer acquisition times (Supplementary Fig. 8).

Several features of the [$^{13}$C]methyl-$\beta_2$AR NMR spectrum are notable (Fig. 2a). The sharpest peak is assigned to the dimethyl-amino terminus based on protease digestion (Fig. 2b and Supplementary Fig 9). The remaining peaks are assigned to dimethyllysines. The region is dominated by a cluster of overlapping peaks (centered at $^1$H chemical shift 2.8 ppm) attributed to solvent exposed, highly mobile lysines. The intensity of this cluster is reduced by ≈50% following mutation of seven cytoplasmic lysines to arginine (Fig. 2b and Supplementary Fig. 10). Two broad dimethyllysine peaks are shifted upfield in the $^1$H dimension (Fig. 2a, Peaks 1 and 2). These peaks represent the two [$^{13}$C]methyl groups on Lys305, as determined by mutation of Lys305 to Arg (Fig. 2c and Supplementary Fig. 10). The fine structure features in Peaks 1 and 2 might suggest conformational heterogeneity; however, they are most likely due to relatively low signal-to-noise ratios and subtle baseline distortions.

Lys305 is the only lysine that forms a salt bridge in the $\beta_2$AR crystal structure, consistent with the unique chemical shifts of Peaks 1 and 2. The presence of two peaks implies that the two methyl groups on Lys305 exist in non-equivalent chemical environments21,22,23. The two peaks merge under conditions of increased temperature and ionic strength, presumably due to weakening of the salt bridge (Supplementary Fig. 11). Reduction of the disulfide

bonds stabilizing ECL2 in the $\beta_2$AR abolishes the Lys305 peaks (Supplementary Fig. 12), demonstrating that the salt bridge is sensitive to conformational changes in the ECS. Taken as a whole, these data show that the Lys305-Asp192 salt bridge is formed in solution as well as in crystal lattices for carazolol-bound $\beta_2$AR2,24. This conclusion is further supported by measurements of $^{13}$C transverse relaxation ($T_2$) times indicating restricted motion of Lys305 compared with other $\beta_2$AR lysines (Supplementary Fig. 13 and Supplementary Table 3).

The Lys305 peaks are a probe for conformational changes in the receptor ECS. Both peaks are present in the NMR spectrum of unliganded $\beta_2$AR indicating that the Lys305-Asp192 salt bridge also forms in the basal state (Fig. 3a). Two differences are seen relative to the carazolol-bound state (Fig. 3b). First, Peaks 1 and 2 have a larger upfield shift in the $^1$H dimension. Second, the $^{13}$C chemical shift separation between Peaks 1 and 2 is increased. These data show that carazolol binding alters the chemical environment around Lys305, demonstrating a change in the ECS. In contrast to inverse agonists, neutral antagonists (e.g., alprenolol) do not alter basal receptor activity. As might be predicted based on ligand efficacy, NMR detects no difference in Lys305 chemical shifts between unliganded and alprenolol-bound $\beta_2$AR (Fig. 3c).

The inverse agonist-induced conformational change (Fig. 3) likely involves Phe193 in ECL2 (Fig. 1b), which forms a favorable edge-to-face interaction with the tricyclic aromatic ring of carazolol in the $\beta_2$AR crystal structure1. Nearly identical interactions are observed with other inverse agonists: Phe193 and timolol in $\beta_2$AR24, and the homologous Phe201 and cyanopindolol in $\beta_1$AR5. By contrast, alprenolol has a single aromatic ring that cannot interact strongly with Phe193 when docked at the carazolol position. Molecular dynamics simulations show that Phe193 adopts the trans conformation pointing toward TM5 in the presence of carazolol, but has increased mobility and is able to assume multiple conformations in the alprenolol-bound state (Supplementary Fig. 14). Phe193 can form close encounters (< 5 Å) with the Lys305 amine when alprenolol is bound. Therefore, the observed upfield chemical shift change of Peaks 1 and 2 in alprenolol-bound receptor relative to carazolol-bound receptor is most likely due to aromatic ring current effects, although we cannot exclude other changes in ECS conformation.

Agonists induce ECS conformational changes that differ from inverse agonists. Adding formoterol, a $\beta_2$AR agonist with nanomolar affinity, attenuates the Lys305 resonances (Fig. 4a, b). The effect is titratable (Supplementary Fig. 15) and reverses when formoterol is exchanged to carazolol by dialysis (Fig. 4c). Attenuation of Lys305 resonances was also observed with another, structurally distinct high-affinity agonist (Supplementary Fig. 16). These NMR data suggest that the Lys305-Asp192 salt bridge is weakened in the $\beta_2$AR active state. Loss of interaction with Asp192 would abolish the unique chemical environment of Lys305. Based on the $\beta_2$AR crystal structure, we estimate that a distance increase of 2.9 Å between the C-alpha carbons of Asp192 and Lys305 is the minimum needed to disrupt the geometrical criteria for a salt bridge established by Kumar and Nussinov25. At equilibrium, the fraction of Lys305 liberated from the salt bridge would be indistinguishable from solvent-exposed lysines (at 2.8 ppm $^1$H chemical shift), explaining the absence of any new peaks. Alternatively, if agonists induce conformational fluctuations on the millisecond time scale, line broadening would attenuate the signal for Lys305. In

either case, we interpret the formoterol-induced conformational change as a relative motion between ECL3-TM7 and ECL2. Conformational changes involving ECL2 are compatible with circular dichroism experiments demonstrating agonist induced changes in the extracellular disulfide bond linking ECL2 and TM3 in the 5-$HT_{4(a)}$ receptor26.

Based on our NMR results and computational modeling, we propose that the extracellular ends of TMs 6 and 7 move upon activation (Fig. 4d). Briefly, formoterol-activated $\beta_2$AR was modeled based on the crystal structure of ligand-free opsin9 and a relaxed conformation of the highly distorted Pro288$^{6.50}$-induced kink (Supplementary Fig. 17). In this active state model, an inward movement at the extracellular end of TM6 permits the known interaction between Asn293$^{6.55}$ and the chiral β-hydroxyl of the agonist27. This motion, simultaneous with outward motion at the intracellular end of TM6 towards TM59, agrees with the activation model derived from engineering GPCRs with metal ion binding sites28,29. The TM6 motion necessitates a lateral displacement of TM7 that reorients the Lys305$^{7.32}$ salt bridge in agreement with NMR spectroscopy (Fig. 4). Inverse agonists may function in part by stabilizing bulky hydrophobic interactions with Phe193$^{ECL2}$ that block TM6 motion.

In summary, NMR spectroscopy can be used to investigate structural changes in GPCRs, although the isotopic labeling methods employed here are limited to monitoring changes in the environment and dynamics of accessible lysine side chains. We provide direct biophysical evidence for three distinct conformations of the $\beta_2$AR extracellular surface: one for an unliganded receptor or a neutral antagonist, one for an inverse agonist, and one for an agonist (Fig. 4e). These conformations correspond to distinct functional behavior. Unliganded and alprenolol-bound $\beta_2$AR are both able to couple to Gs, consistent with the basal activity of the receptor and the efficacy of alprenolol (neutral antagonist). In contrast, the inverse agonist carazolol prevents receptor-Gs coupling. Finally, agonists promote the strongest coupling. Ligands binding to the extracellular surface could therefore modulate receptor function, either by influencing the binding of orthosteric ligands or by direct allosteric modulation of cytoplasmic domain conformation (Supplementary Fig. 1). While the specific salt bridge used to monitor these conformations may not be present in other GPCRs, it is ideally positioned to monitor ECS conformations in the $\beta_2$AR, and it is likely that our findings regarding ligand-induced changes in the ECS are relevant for other Family A GPCRs.

## Methods Summary

### NMR spectroscopy of [$^{13}$C]-methyl $\beta_2$AR

Human $\beta_2$AR, tagged with an N-terminal FLAG-TEV sequence, and truncated after residue Gly365 ($\beta_2$AR365, Supplementary Fig. 2) was expressed in Sf9 insect cells using recombinant baculovirus. Sf9 cell membranes were solubilized with dodecylmaltoside and purified by sequential antibody affinity and alprenolol affinity chromatography, as previously described3. $^{13}$C methyl labeling was performed by sequentially adding excess sodium cyanoborohydride followed by [$^{13}$C]-formaldehyde to purified $\beta_2$AR. Methylation reagents were removed by extensive dialyisis (unliganded $\beta_2$AR) or by anion exchange chromatography (carazolol-bound $\beta_2$AR). For NMR spectroscopy, [$^{13}$C]-methyl $\beta_2$AR was dialyzed against buffer containing 20 mM HEPES (pH 7.4), 100 mM NaCl, and 0.1%

dodecylmaltoside prepared in 98% $D_2O$ and concentrated to a final concentration of 50 to 200 μM. Two-dimensional $^1H$-$^{13}C$ correlation spectra of [$^{13}C$]-methyl $\beta_2$AR were recorded at 800 MHz for approximately eight hours (HSQC) or 24 hours (STD-filtered HMQC) at 25 °C. Both pulse sequences used WATERGATE water suppression. See Supplementary Fig. 8 for all parameters and full details of NMR spectroscopy.

### Crystal structure of [$^{13}C$]methyl-$\beta_2$AR / Fab5 complex

[$^{13}C$]methyl-$\beta_2$AR / Fab5 complex was prepared and crystallized as previously described3. Diffraction images were obtained on a microfocus beam line, and the structure solved by molecular replacement using $\beta_2$AR-Fab5 (2R4R) as a search model.

**Full Methods** and any associated references are available in the online version of the paper at www.nature.com/nature.

## Methods

### Buffers

Buffer A is 20 mM HEPES (pH 7.4), 100 mM NaCl, 0.1% dodecylmaltoside. Buffer B is 20 mM HEPES (pH 7.4), 80 mM NaCl, 0.1% dodecylmaltoside. Buffer C is 20 mM HEPES (pH 7.4), 60 mM NaCl, 0.1% dodecylmaltoside. Buffer D is 20 mM HEPES (pH 7.4), 350 mM NaCl, 0.1% dodecylmaltoside. Buffer E is Buffer A + $CaCl_2$ (2 mM), 0.01% cholesterol hemisuccinate. Buffer F is Buffer A + EDTA (5 mM), 0.01% cholesterol hemisuccinate

### Preparation of modified $\beta_2$ adrenergic receptors for NMR

The coding sequence of wild-type human $\beta_2$ adrenergic receptor ($\beta_2$AR) was cloned into the pFastBac1 Sf9 insect cell expression vector (Invitrogen) and modified as previously described3. For small-scale expression trials (≤ 1 L), recombinant baculovirus was made using the Bac-to-Bac system (Invitrogen). For large NMR and crystallography-scale expressions, the $\beta_2$AR cDNA was subcloned into the pVL1392 transfer vector and recombinant baculovirus made using the BestBac system (Expression Systems, Woodland, CA). All cells were cultured in ESF 921 insect cell medium (Expression Systems). $\beta_2$AR365 (Supplementary Fig. 2) was expressed in Sf9 insect cells infected with baculovirus and solubilized in 1% *n*-dodecyl-β-D-maltopyranoside (dodecylmaltoside, Anatrace) according to previously described methods31. M1 FLAG affinity chromatography (Sigma) was used as the initial purification step. FLAG-purified receptor was treated with 100 μM tris(2-carboxyethyl)phosphine followed by two additions of 2 mM iodoacetamide (two times, for 1 hr each on ice) to alkylate reactive cysteines that can cause disulfide aggregation (these and all other reagents were from Sigma unless otherwise noted). Alternatively, $\beta_2$AR365 was labeled with the cysteine-reactive fluorophore monobromobimane prior to alkylation, to assess ligand-induced conformational changes32. Alkylation was quenched by addition of 5 mM L-cysteine. Functional $\beta_2$AR365 was then selectively purified by alprenolol-Sepharose chromatography31. The next preparation steps varied depending on the particular NMR sample being prepared.

### Preparation of Carazolol-bound [$^{13}$C]-methyl $\beta_2$AR365

$\beta_2$AR365 (purified by alprenolol-Sepharose) was reductively methylated by sequentially adding 10 mM freshly prepared sodium cyanoborohydride, briefly vortexing, and then adding 10 mM $^{13}$C-enriched (99%) formaldehyde (CLM-806-1, Cambridge Isotope Labs). We feel that the order of reagent addition is important. We prefer to first set a reducing environment in solution to avoid protein cross-linking by formaldehyde. The reductive methylation reaction was then allowed to proceed overnight (minimum 8 hr) at 4 °C with nutation. A second addition of sodium cyanoborohydride and [$^{13}$C]formaldehyde was made exactly as before, followed by another 4 hr incubation at 4 °C. [$^{13}$C]-methyl $\beta_2$AR365 was then dialysed extensively against Buffer A + 1 μM carazolol, to remove unreacted methylation reagents and exchange alprenolol for carazolol.

Reductive methylation destroys the antigenicity of the M1 FLAG epitope, so we could not use a second M1 FLAG affinity step to concentrate [$^{13}$C]methyl-$\beta_2$AR365 to NMR concentrations. The receptor was instead loaded onto Q Sepharose anion exchange resin equilibrated in Buffer B. We estimate the capacity of Q Sepharose to be ≈2.5 mg [$^{13}$C]methyl-$\beta_2$AR365 per mL of resin. Binding is largely mediated through the acidic FLAG epitope (amino acid sequence DYKDDDDA), since TEV-cleaved $\beta_2$AR365 does not bind tightly to Q Sepharose resin. The column was then washed with three column volumes of Buffer C + 1 μM Carazolol, and eluted with Buffer D + 1 μM Carazolol. A one-tenth volume of a saturated cholesterol hemisuccinate solution in Buffer A was added to the eluate to enhance receptor stability. [$^{13}$C]methyl $\beta_2$AR365 typically eluted at a concentration of ≈100 μM as determined by measurement of carazolol fluorescence33. N-linked glycosylations were removed by treatment with PNGase F (750 units / mg of $\beta_2$AR365) for 1 hr at room temperature (New England BioLabs). The sample was dialyzed extensively against Buffer A + 100 nM carazolol, followed by two dialysis steps against a small volume (≈25 mL) of Buffer A prepared in 98% $D_2O$ (Cambridge Isotope Labs) + 100 nM carazolol. Receptor was then concentrated to ≈200 μM with a 100 kDa molecular weight cutoff (MWCO) Vivaspin concentrator (Vivascience). It is important to wash the concentrator membrane extensively with water, followed by $D_2O$, to remove as much glycerol as possible that may interfere with NMR spectroscopy.

Final NMR samples (≈270 μL) were loaded into Shigemi microtubes susceptibility matched to $D_2O$ (Shigemi Inc., Allison Park, PA) and sealed. Carazolol-bound [$^{13}$C]-methyl $\beta_2$AR samples remained stable for over four months with no visible precipitation, degradation of NMR spectral quality, or decrease in bound carazolol fluorescence. This method was used to prepare the samples shown in Main Text Fig. 2a and Supplementary Figs. 7-9 and 13.

### Preparation of unliganded [$^{13}$C]-methyl $\beta_2$AR365

$\beta_2$AR365 (purified by alprenolol-Sepharose, 2 mM $CaCl_2$ added) was loaded directly onto M1 resin for a second FLAG affinity step. After loading, the column was washed at 10 mL/hr with six column volumes of Buffer E + 30 μM atenolol. Atenolol is an antagonist with relatively low affinity for the $\beta_2$AR ($K_d$ ≈ 1 μM)34. This wash step was included to displace the higher affinity antagonist alprenolol ($K_d$ ≈ 1 nM) from $\beta_2$AR365 by competition. The FLAG M1 column was then washed extensively with Buffer E to remove

atenolol and guarantee that all bound ligand was removed. Unliganded $\beta_2$AR365 was then eluted with Buffer F + FLAG peptide (100 μg/mL). Glycosylations were removed by treatment with PNGase F as described above. Receptor was dialyzed against Buffer A using a 20 kDa MWCO dialysis cassette (Slide-A-Lyzer, Pierce) to ensure removal of FLAG peptide prior to [$^{13}$C]methylation. FLAG peptide (amino acid sequence DYKDDDDK) has three primary amines that can be [$^{13}$C]methylated and cause undesirable NMR background.

Unliganded $\beta_2$AR365 was reductively methylated (as described above), dialyzed against Buffer A to remove labeling reagents, dialyzed against Buffer A prepared in 98% $D_2O$, and concentrated for NMR as described above. This method was used to prepare the samples shown in Main Text Fig. 3 and 4, and Supplementary Figs. 12 and 15. Ligand additions to unliganded [$^{13}$C]methyl-365N NMR samples were made from ligand stocks dissolved in perdeuterated dimethyl $d_6$-sulfoxide (DLM-10-10, Cambridge Isotope Labs). (R,R)-Formoterol was a kind gift of Sepracor (Marlborough, MA).

## Preparation of Carazolol-bound [$^{13}$C]methyl-$\beta_2$AR365 mutants for Lysine-305 peak assignment

To facilitate assignment of dimethyllysine Peaks 1 and 2 (*Main Text*, Fig. 2a), we developed a small-scale expression and purification technique that yields an NMR sample of carazolol-bound $\beta_2$AR365 (≈2-3 mg) from 1-2 liters of Sf9 cells. We modified $\beta_2$AR365 to include a carboxyl terminus hexahistidine tag for nickel affinity chromatography31. Six histidine codons were added to the $\beta_2$AR365 cDNA between the Gly365 and STOP codons ($\beta_2$AR365-His).

To maximize yield of $\beta_2$AR365-His, we directly added 200 nM carazolol to the culture media at the time of baculovirus infection. Buffers for all subsequent purification steps also included a minimum of 200 nM carazolol. We have observed that inverse agonists improve cell surface expression and help to stabilize the receptor during solubilization. However, the affinity of $\beta_2$AR for carazolol ($K_d$ < 0.1 nM) is sufficiently high that binding is essentially irreversible. This precludes the use of alprenolol-Sepharose chromatography as a functional purification step. Instead, $\beta_2$AR365-His was first purified by FLAG affinity chromatography. Reactive cysteines were alkylated as described above and the protein was dialyzed extensively against Buffer A to remove FLAG peptide. Reductive methylation was performed as described above. [$^{13}$C]methyl-$\beta_2$AR365-His was then purified by nickel affinity chromatography (Chelating Sepharose Fast Flow, GE Healthcare) as previously described31. Final NMR dialysis and concentration was performed as described above. This method was used to prepare the samples shown in Main Text Fig. 2b-c, and Supporting Figs. 10 and 11.

## Crystallographic data collection and processing

Crystals of reductively methylated $\beta_2$AR365-Fab5 complex were generated essentially as described in Rasmussen *et al.* and were isomorphous to the non-methylated receptor-Fab5 complex3. Data collection was carried out using the 10 μm collimated microfocus beamline 23ID-B of the APS. A data set comprising 316° of oscillation data was obtained from a single crystal (see Supplementary Table 2). Due to radiation damage, only 5 to 10° of data

(1° per frame) could be measured before the crystal was translated to a new position. Data were processed with HKL200035. Similar to the previous $\beta_2$AR24/365–Fab5 complex data reduction, global post-refinement of the unit cell parameters was not performed. Rather, the unit cell parameters were obtained from indexing and refinement from one wedge of data, and were subsequently used for processing the remaining data without unit cell constant refinement.

### Structure solution and refinement

The structure of the methylated $\beta_2$AR365–Fab5 complex was solved by initially performing rigid body refinement in CNS36 using the unmethylated $\beta_2$AR24/365–Fab5 complex structure (PDB code 2R4S) as a single rigid body. This gave $R$ and $R_{free}$ values of 0.358 and 0.348, respectively. Multiple rounds of manual rebuilding, positional refinement, grouped temperature factor refinement, and TLS refinement were performed using the PHENIX package37, bringing $R$ and $R_{free}$ values down to 0.233 and 0.274, respectively. As in the previous $\beta_2$AR24/365–Fab5 complex refinement3, only those residues that could be unambiguously assigned were included in the final model. In addition to the residues present in the $\beta_2$AR24/365–Fab5 structure (PDB 2R4S), receptor residues 35-36, 91, and 307-310 were included in the methylated $\beta_2$AR365–Fab5 model. The following receptor residues were modeled as alanine due to insufficient electron density to model full sidechains: 36, 39, 42, 49, 53, 55, 63, 69, 77, 112, 114, 120, 122, 131, 147, 156, 209, 227, 232, 263, 279, 287, 308, 309, 321, 324, 326, 332.

## Supplementary Material

Refer to Web version on PubMed Central for supplementary material.

## Acknowledgements

We acknowledge support from National Institutes of Health Grants NS028471 (B.K.K.) and GM56169 (W.I.W.), the Stanford Medical Scientist Training Program (M.P.B), the Lundbeck Foundation (S.G.F.R.), the University of Copenhagen and 7TM Pharma (R.N.), and the Instituto de Salud Carlos III (L.P.).

## References

1. Rosenbaum DM, et al. GPCR engineering yields high-resolution structural insights into beta2-adrenergic receptor function. Science. 2007; 318:1266–73. [PubMed: 17962519]
2. Cherezov V, et al. High-resolution crystal structure of an engineered human beta2-adrenergic G protein-coupled receptor. Science. 2007; 318:1258–65. [PubMed: 17962520]
3. Rasmussen SG, et al. Crystal structure of the human beta2 adrenergic G-protein-coupled receptor. Nature. 2007; 450:383–7. [PubMed: 17952055]
4. Jaakola VP, et al. The 2.6 angstrom crystal structure of a human A2A adenosine receptor bound to an antagonist. Science. 2008; 322:1211–7. [PubMed: 18832607]
5. Warne T, et al. Structure of a beta1-adrenergic G-protein-coupled receptor. Nature. 2008; 454:486–91. [PubMed: 18594507]
6. Kobilka BK, Deupi X. Conformational complexity of G-protein-coupled receptors. Trends Pharmacol Sci. 2007; 28:397–406. [PubMed: 17629961]
7. Farrens DL, Altenbach C, Yang K, Hubbell WL, Khorana HG. Requirement of rigid-body motion of transmembrane helices for light activation of rhodopsin. Science. 1996; 274:768–70. [PubMed: 8864113]

8. Altenbach C, Kusnetzow AK, Ernst OP, Hofmann KP, Hubbell WL. High-resolution distance mapping in rhodopsin reveals the pattern of helix movement due to activation. Proc Natl Acad Sci U S A. 2008; 105:7439–44. [PubMed: 18490656]
9. Park JH, Scheerer P, Hofmann KP, Choe HW, Ernst OP. Crystal structure of the ligand-free G-protein-coupled receptor opsin. Nature. 2008; 454:183–7. [PubMed: 18563085]
10. Scheerer P, et al. Crystal structure of opsin in its G-protein-interacting conformation. Nature. 2008; 455:497–502. [PubMed: 18818650]
11. Ghanouni P, et al. Functionally different agonists induce distinct conformations in the G protein coupling domain of the beta(2) adrenergic receptor. J Biol Chem. 2001; 276:24433–24436. [PubMed: 11320077]
12. Swaminath G, et al. Probing the beta2 adrenoceptor binding site with catechol reveals differences in binding and activation by agonists and partial agonists. J Biol Chem. 2005; 280:22165–71. [PubMed: 15817484]
13. Yao X, et al. Coupling ligand structure to specific conformational switches in the beta2-adrenoceptor. Nat Chem Biol. 2006; 2:417–22. [PubMed: 16799554]
14. Ahuja S, et al. Helix movement is coupled to displacement of the second extracellular loop in rhodopsin activation. Nat Struct Mol Biol. 2009; 16:168–75. [PubMed: 19182802]
15. Conn PJ, Christopoulos A, Lindsley CW. Allosteric modulators of GPCRs: a novel approach for the treatment of CNS disorders. Nat Rev Drug Discov. 2009; 8:41–54. [PubMed: 19116626]
16. Ballesteros JA, Weinstein H. Integrated methods for the construction of three-dimensional models and computational probing of structure-function relations in G-protein coupled receptors. Methods Neurosci. 1995; 25:366–428.
17. Nygaard R, Frimurer TM, Holst B, Rosenkilde MM, Schwartz TW. Ligand binding and micro-switches in 7TM receptor structures. Trends Pharmacol Sci. 2009; 30:249–59. [PubMed: 19375807]
18. Zhang M, Vogel HJ. Determination of the side chain pKa values of the lysine residues in calmodulin. J Biol Chem. 1993; 268:22420–8. [PubMed: 8226750]
19. Tugarinov V, Hwang PM, Ollerenshaw JE, Kay LE. Cross-correlated relaxation enhanced 1H[bond]13C NMR spectroscopy of methyl groups in very high molecular weight proteins and protein complexes. J Am Chem Soc. 2003; 125:10420–8. [PubMed: 12926967]
20. Jentoft JE, Jentoft N, Gerken TA, Dearborn DG. 13C NMR studies of ribonuclease A methylated with [13C]Formaldehyde. J Biol Chem. 1979; 254:4366–70. [PubMed: 571438]
21. Gerken TA, Jentoft JE, Jentoft N, Dearborn DG. Intramolecular interactions of amino groups in 13C reductively methylated hen egg-white lysozyme. J Biol Chem. 1982; 257:2894–900. [PubMed: 7061454]
22. Sherry AD, Teherani J. Physical studies of 13C-methylated concanavalin A. pH- and Co2+-induced nuclear magnetic resonance shifts. J Biol Chem. 1983; 258:8663–9. [PubMed: 6863304]
23. Abraham SJ, Hoheisel S, Gaponenko V. Detection of protein-ligand interactions by NMR using reductive methylation of lysine residues. J Biomol NMR. 2008; 42:143–8. [PubMed: 18819009]
24. Hanson MA, et al. A specific cholesterol binding site is established by the 2.8 A structure of the human beta2-adrenergic receptor. Structure. 2008; 16:897–905. [PubMed: 18547522]
25. Kumar S, Nussinov R. Relationship between ion pair geometries and electrostatic strengths in proteins. Biophys J. 2002; 83:1595–612. [PubMed: 12202384]
26. Baneres JL, et al. Molecular characterization of a purified 5-HT4 receptor: a structural basis for drug efficacy. J Biol Chem. 2005; 280:20253–60. [PubMed: 15774473]
27. Wieland K, Zuurmond HM, Krasel C, Ijzerman AP, Lohse MJ. Involvement of Asn-293 in stereospecific agonist recognition and in activation of the beta 2-adrenergic receptor. Proc Natl Acad Sci U S A. 1996; 93:9276–81. [PubMed: 8799191]
28. Elling CE, et al. Metal ion site engineering indicates a global toggle switch model for seven-transmembrane receptor activation. J Biol Chem. 2006; 281:17337–46. [PubMed: 16567806]
29. Schwartz TW, Frimurer TM, Holst B, Rosenkilde MM, Elling CE. Molecular mechanism of 7TM receptor activation--a global toggle switch model. Annu Rev Pharmacol Toxicol. 2006; 46:481–519. [PubMed: 16402913]

30. Hubbard SJ, Campbell SF, Thornton JM. Molecular recognition. Conformational analysis of limited proteolytic sites and serine proteinase protein inhibitors. J Mol Biol. 1991; 220:507–30. [PubMed: 1856871]

31. Kobilka BK. Amino and carboxyl terminal modifications to facilitate the production and purification of a G protein-coupled receptor. Anal Biochem. 1995; 231:269–71. [PubMed: 8678314]

32. Yao XJ, et al. The effect of ligand efficacy on the formation and stability of a GPCR-G protein complex. Proc Natl Acad Sci U S A. 2009; 106:9501–9506. [PubMed: 19470481]

33. Tota MR, Strader CD. Characterization of the binding domain of the beta-adrenergic receptor with the fluorescent antagonist carazolol. Evidence for a buried ligand binding site. J Biol Chem. 1990; 265:16891–7. [PubMed: 1976626]

34. Baker JG. The selectivity of beta-adrenoceptor antagonists at the human beta1, beta2 and beta3 adrenoceptors. Br J Pharmacol. 2005; 144:317–22. [PubMed: 15655528]

35. Otwinowski Z, Minor W. Processing of X-ray diffraction data collected in oscillation mode. Macromolecular Crystallography, Pt A. 1997; 276:307–326.

36. Brunger AT, et al. Crystallography & NMR system: A new software suite for macromolecular structure determination. Acta Crystallographica Section D-Biological Crystallography. 1998; 54:905–921.

37. Adams PD, et al. PHENIX: building new software for automated crystallographic structure determination. Acta Crystallographica Section D-Biological Crystallography. 2002; 58:1948–1954.

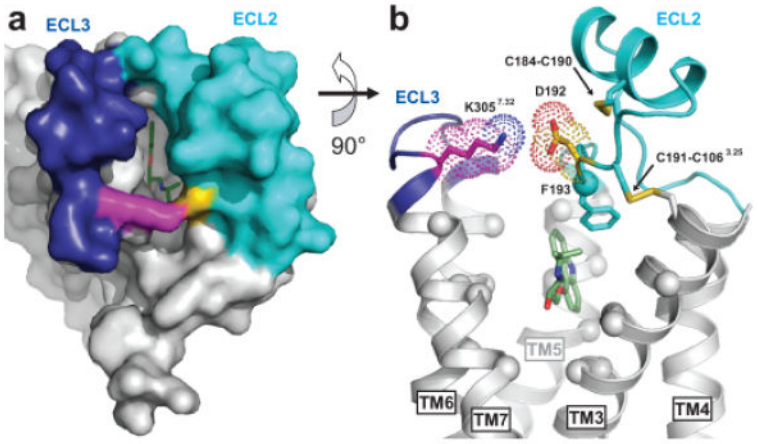


**Figure 1. Extracellular domains of carazolol-bound $\beta_2$AR (PDB: 2RH1)**

**a,** The extracellular surface (ECS) of $\beta_2$AR showing extracellular loop 2 (ECL2, cyan, Met171-Ala198), extracellular loop 3 (ECL3, dark blue, His296-Glu306), Lys305$^{7.32}$ (magenta), Asp192 (yellow), and inverse agonist carazolol (green). ECL1 (Met96-Phe108) is part of the ECS but is not colored. **b,** Intramolecular and ligand binding interactions. Spheres indicate the alpha carbons of residues in direct contact with carazolol (at least one atom within 4 Å distance). Disulfide bonds are shown as yellow sticks. Other colors are the same as in **a.** Transmembrane helices 1 and 2 removed for clarity. D192 and K305 form the only lysine salt bridge observed in the crystal structure. The solvent accessibility of D192 and K305 was calculated with the NACCESS program (Hubbard & Thornton). The relative accessibilities of D192 and K305 are 35% and 75%, respectively, compared to the accessibility of that residue type in an extended Ala-x-Ala tripeptide30.

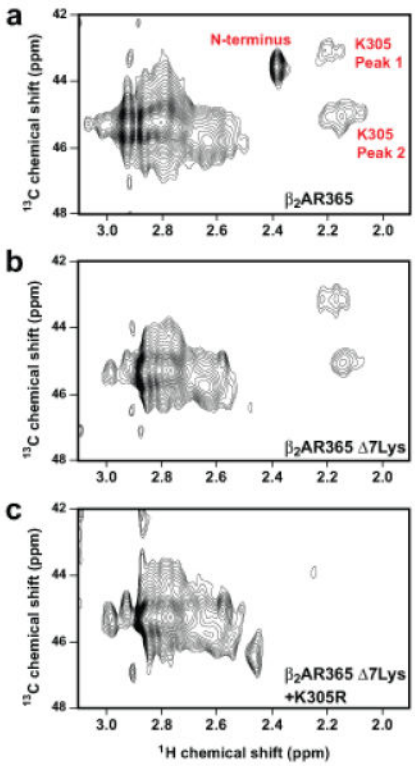


**Figure 2. Dimethyllysine NMR spectroscopy of [$^{13}$C]methyl-$\beta_2$AR and assignment of Lys305**

**a,** Dimethylamine region of STD-filtered HC-HMQC spectrum of carazolol-bound $\beta_2$AR365, containing 14 Lys and amino terminal FLAG-TEV sequence (Supplementary Fig. 2). **b,** Spectrum of $\beta_2$AR365 with seven cytoplasmic Lys to Arg mutations ($\beta_2$AR365 Δ7Lys) and the amino terminus removed by TEV proteolysis. **c,** Spectrum of $\beta_2$AR365 Δ7Lys plus the Lys305Arg mutation and the amino terminus removed by TEV proteolysis.

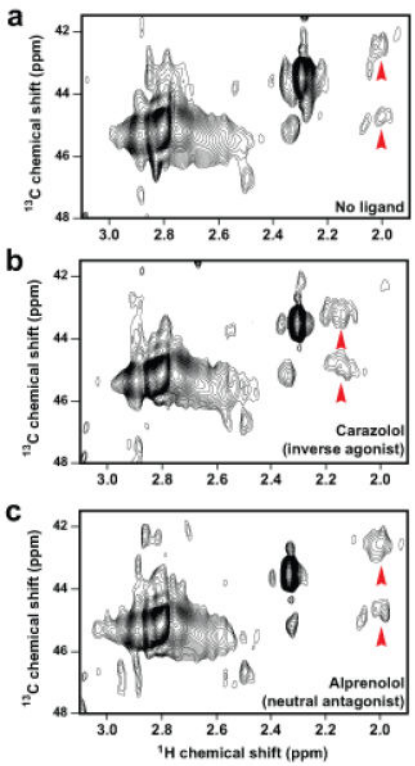


**Figure 3. Effect of inverse agonist and antagonist on the [$^{13}$C]dimethyl-Lys305 NMR resonances**

HSQC spectra of **a,** unliganded $\beta_2$AR (≈60 μM), **b,** $\beta_2$AR bound to inverse agonist carazolol and **c,** $\beta_2$AR bound to neutral antagonist alprenolol.

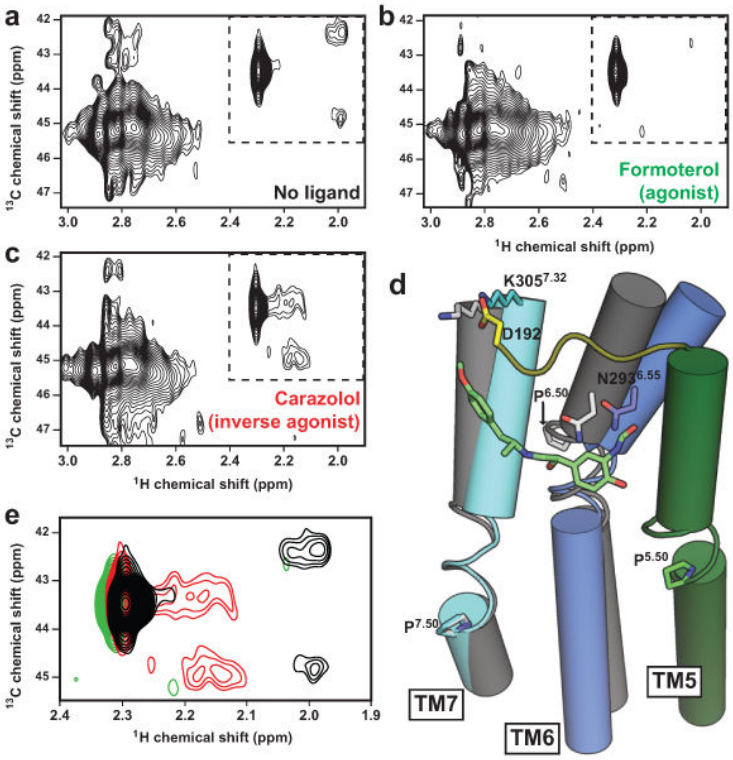


**Figure 4. Activation of $\beta_2$AR by formoterol**

STD-filtered HMQC spectra of **a,** unliganded $\beta_2$AR (≈60 μM), **b,** the same sample bound to a saturating concentration (320 μM) of agonist (R,R)-formoterol, and **c,** the same sample after exchanging formoterol for inverse agonist carazolol by dialysis. **d,** Model of $\beta_2$AR activation by formoterol (see Supplementary Fig. 16). Colored helices, loops, and side chains represent the carazolol-bound crystal structure (PDB: 2RH1). Gray helices and white side chains indicate the active state model. Green sticks indicate (R,R)-formoterol and yellow indicates ECL2. **e,** Overlay of spectra corresponding to dashed regions shown in panels **a-c**. The spectrum of unliganded $\beta_2$AR from panel **a** is shown in black, agonist-bound $\beta_2$AR from panel **b** in green, and inverse agonist-bound $\beta_2$AR from panel **c** in red.